

Wind turbine wake detection with a single Doppler wind lidar

H Wang and R J Barthelmie

Sibley School of Mechanical and Aerospace Engineering, Cornell University, USA

E-mail: hw524@cornell.edu

Abstract. Using scanning lidar wind turbine wakes can be probed in three dimensions to produce a wealth of temporally and spatially irregular data that can be used to characterize the wakes. Unlike data from a meteorological mast or upward pointing lidar, the spatial coordinates of the measurements are not fixed and the location of the wake also varies in three dimensions. Therefore the challenge is to provide automated detection algorithms to identify wakes and quantify wake characteristics from this type of dataset. Here an algorithm is developed and evaluated on data from a large wind farm in the Midwest. A scanning coherent Doppler wind lidar was configured to measure wind speed in the wake of a continuously yawing wind turbine for two days during the experiment and wake profiles were retrieved with input of wind direction information from the nearby meteorological mast. Additional challenges to the analysis include incomplete coverage of the entire wake due to the limited scanning domain, and large wind shear that can contaminate the wake estimate because of the height variation along the line-of-sight. However, the algorithm developed in this paper is able to automatically capture wakes in lidar data from Plan Position Indicator (PPI) scans and the resultant wake statistics are consistent with previous experiment's results.

1 Introduction

Wind turbine wakes are characterized by low wind speed and high turbulence intensity relative to the freestream. As a result, wind turbines in the wake of operating wind turbines can experience reduced power output and enhanced fatigue load [1]. To reduce the adverse effects of wind turbine wakes, accurate wake modelling plays a critical role in wind farm layout and operation optimization, and the accuracy of the wake models needs to be verified with observations [2]. While verification can be performed with in-situ measurements and downscaled experiments in wind tunnels, remote sensing technologies have shown potential in studying wake characteristics and testing wake models in full-scale wind farms. For example, a single coherent Doppler wind lidar (hereafter called lidar) can be used to study the wake recovery and expansion along the downwind distance from the wind turbine under various atmospheric conditions [3]. With two lidars it has been shown that wake has a fast recovery rate in convective atmospheric conditions [4]. Measurements from dual Doppler radars have been used to characterize the complex flow features such as wake merging in a large wind farm [5]. To further explore the potential of lidar for wind turbine wake characterization, this paper presents an experiment designed to test the performance of a single lidar for measuring the wake of a continuously yawing wind turbine. This paper is organized as follows: A brief description of lidar operation principle is given in Section 2, and then followed by the description of the experiment setup in Section 3. The wake profile estimation algorithm is described in Section 4. Section 5 presents the wake characteristics, such as wake deficit and wake width, derived from the lidar measurements. Conclusions are drawn in Section 6.



2 Lidar basics

A lidar only measures the radial velocity at each range gate. The radial velocity (v_R) is the projection of the wind velocity ($\mathbf{v} = [u, v, w]$) on the line-of-sight (LOS) which is the path of the light wave emitted by the lidar (Fig. 1). Mathematically, the radial velocity can be expressed as

$$v_R = u \cos \beta \sin \alpha + v \cos \beta \cos \alpha + w \sin \beta \quad (1)$$

where α and β are the azimuth angle and the elevation angle of the LOS, respectively, and u , v and w are the west-east, south-north and vertical components of the wind velocity. The radial velocity can also be defined in terms of the horizontal wind speed (V) and wind direction (θ_w):

$$v_R = -V \cos \beta \cos(\alpha - \theta_w) + w \sin \beta \quad (2)$$

where $V = \sqrt{u^2 + v^2}$ and $\theta_w = \pi + \arctan(u/v)$. The range gate is the area over which the echo samples are used to estimate the radial velocity, and therefore the measured v_R represents the mean wind condition over the range gate.

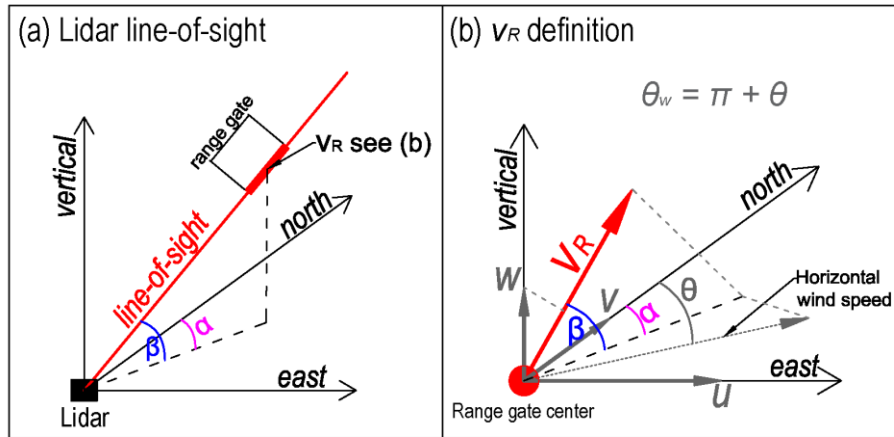


Figure 1. Schematics of (a) the orientation of the lidar line-of-sight in terms of the elevation angle (β) and the azimuth angle (α), and (b) the relationship between the radial velocity (v_R) and the wind velocity ($\mathbf{v} = [u, v, w]$), and the relationship between the radial velocity and the horizontal wind speed and wind direction (θ_w).

3 Experiment setup

This experiment was conducted in a large wind farm in Indiana from 7-20 May 2012 [6]. Results are presented here from a case study on May 16 and 17, 2012 when the wind direction was from the northeast and southeast. A Galion lidar (denoted as Galion hereafter) was deployed on the southwest edge of the wind farm. To probe the wake of the wind turbine denoted as WT2 in Fig. 2, the Galion was configured to perform 3-stack Plan Position Indicator (PPI) scans. Each stack of PPI scans has a fixed elevation angle and varying azimuth angles. The elevation angles were set to 8.0° , 8.5° and 9.0° for the three stacks, respectively. For each PPI stack, the azimuth angle changed from 60° to 90° with 1° increment. The range gate size was 30 m. The wind turbine WT2 has a hub height of 80 m and a rotor diameter of 77 m, and hence it was located between the range gate 17 and 18 of the three PPI stacks (Fig. 2). The Galion's measurement height decreases with decreasing range gate, but it can still detect the wake of WT2 at the range gate 10 which is about 44 m above the ground and higher than the bottom tip of the rotor (41.5 m). An 80-m tall meteorological mast was collocated with the Galion, and the wind direction measured at 77 m height from the meteorological mast are used to estimate the wake profiles from the Galion measurements. In addition, two ZephIR lidars were located about 10 m north of the Galion lidar measuring wind speeds at 40, 80, 120, 160 and 200 m height [6].

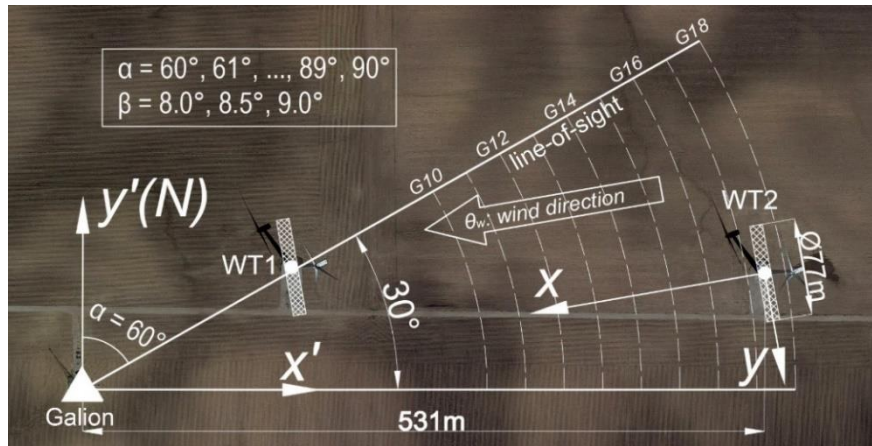


Figure 2. Top view of the locations of the Galion and the two wind turbines (WT1 and WT2), the scanning geometry used to probe the wake of WT2, and the two coordinate systems denoted as $x'-y'$ and $x-y$ (details see 4.2). The azimuth angles (α) and elevation angles (β) used are listed on the upper-left corner. The range gate locations are denoted by the dashed white lines. The underlying wind farm map is from the Google Earth.

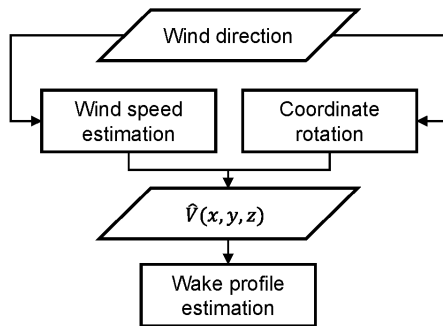


Figure 3. Wake profile estimation algorithm flow chart. The term \hat{V} is the wind speed estimated using the lidar data.

4 Wake profile estimation algorithm

Wake characteristics are quantified by interpolating the wind speed estimated from the measured v_R to the locations of interest in the wake of WT2 using the Gaussian kernel smoother. Wake profiles are estimated for lines parallel to the rotor plane of WT2 at every $0.2D$ distance downwind of WT2, where D is the rotor diameter. The first line is located at $1.0D$ downwind of WT2. The conical surface formed by each PPI stack is treated as a slanted flat surface by ignoring the small curvature on the conical surface. Because of the non-zero elevation angle, the height associated with the estimated wind speed varies across one individual line and among multiple lines for one PPI stack. Wake profiles are estimated from the measured v_R of each PPI stack according to the flow chart shown in Fig. 3. The estimation method requires the wind direction as an input and uses the Gaussian kernel smoother to estimate the wake profiles of WT2. The details of the algorithm are given below.

4.1 Wind direction

The wake profile estimation algorithm requires *a priori* knowledge of the wind direction, which can be obtained from the wind direction measured at the nearby meteorological mast, or estimated from the Galion measurements in the freestream. For this project, the input wind direction is from the wind vane at 77 m height on the meteorological mast. Though wind directions are estimated from the measured radial velocities between the range gate 24 and 28, the estimated wind directions are not reliable because

of the possible wind speed gradient at the edge of the wind farm. Thus, the wind direction estimated from the Galion measurements is not used.

4.2 Coordinate rotation

Two Cartesian coordinate systems are used in this algorithm. The first one is the conventional meteorological coordinate system (x', y') with its origin at the Galion location and x-coordinate and y-coordinate increasing eastward and northward, respectively (Fig. 2). The second one is the streamwise coordinate system (x, y) with its origin at the location of WT2 (Fig. 2). The relationship between the two coordinate systems is a function of the wind direction θ_w :

$$x = x' \cos(1.5\pi - \theta_w) + y' \sin(1.5\pi - \theta_w) \quad (3)$$

$$y = y' \cos(1.5\pi - \theta_w) - x' \sin(1.5\pi - \theta_w) \quad (4)$$

Noting here we assume the rotor axis is parallel to the wind direction (i.e. no yaw error).

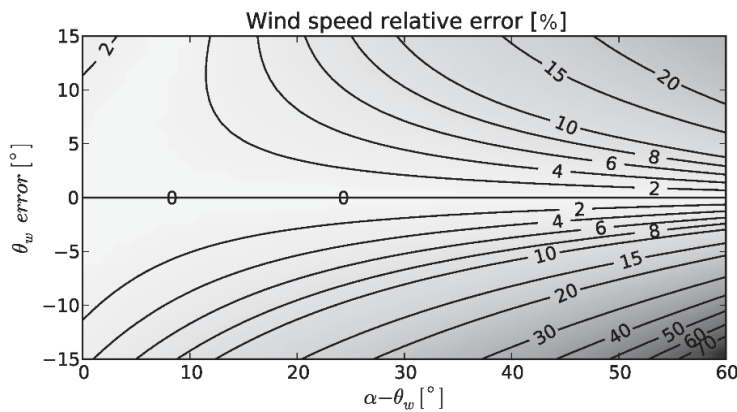


Figure 4. Contours of the wind speed relative error as a function of the wind direction (θ_w) error and the angle between the LOS and the wind direction ($\alpha - \theta_w$), when Eq. (5) is used to estimate the wind speed.

4.3 Wind speed estimation

When the vertical wind speed w is close to zero or the elevation angle β is small, the term $w \sin \beta$ in Eq. (2) can be dropped. Then the horizontal wind speed (V) can be calculated by rearranging Eq. (2) as

$$V = -\frac{v_R}{\cos \beta \cos(\alpha - \theta_w)} \quad (5)$$

An incorrect θ_w can introduce an error in the estimate of V , and the error is a function of both the wind direction error and the angle between the LOS and the wind direction, namely, $\alpha - \theta_w$. The error is small and insensitive to the wind direction error when $(\alpha - \theta_w)$ is small (Fig. 4). When $(\alpha - \theta_w) = 60^\circ$, the wind direction needs to be accurate within $\pm 5^\circ$ in order to ensure that the relative error of the estimated wind speed $< 10\%$.

4.4 Wake profile estimation

For each PPI stack, wake profiles are estimated for lines that are parallel to the rotor plane of WT2 at every 0.2D downwind of WT2. The estimation starts at 1.0D and ends when the x-axis in Fig. 2 is out of the scanning domain. The wind speed at a point of interest is estimated as the weighted average of all available wind speeds estimated with Eq. (5) from one PPI stack. The weight function is given by

$$w_{gt}(x, y) = \exp\left(-\frac{l^2}{2L^2}\right) \quad (6)$$

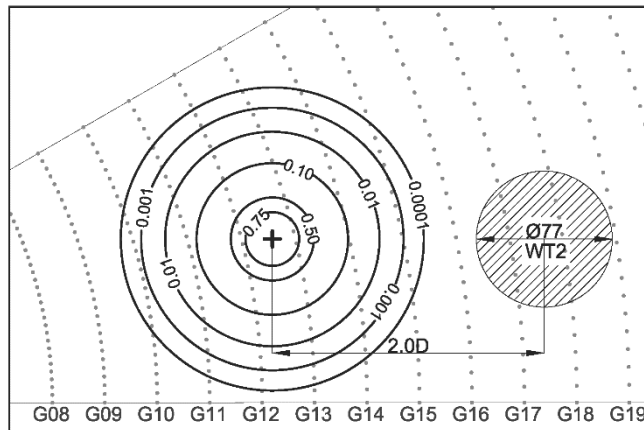


Figure 5. Contours of the weight used to calculate the wind speed at a point (dark cross) two rotor diameters (2.0D) downwind of WT2 using Eq. (6). The gray circles are the Galion range gate locations, and the range gates are indexed by the numbers at the bottom.

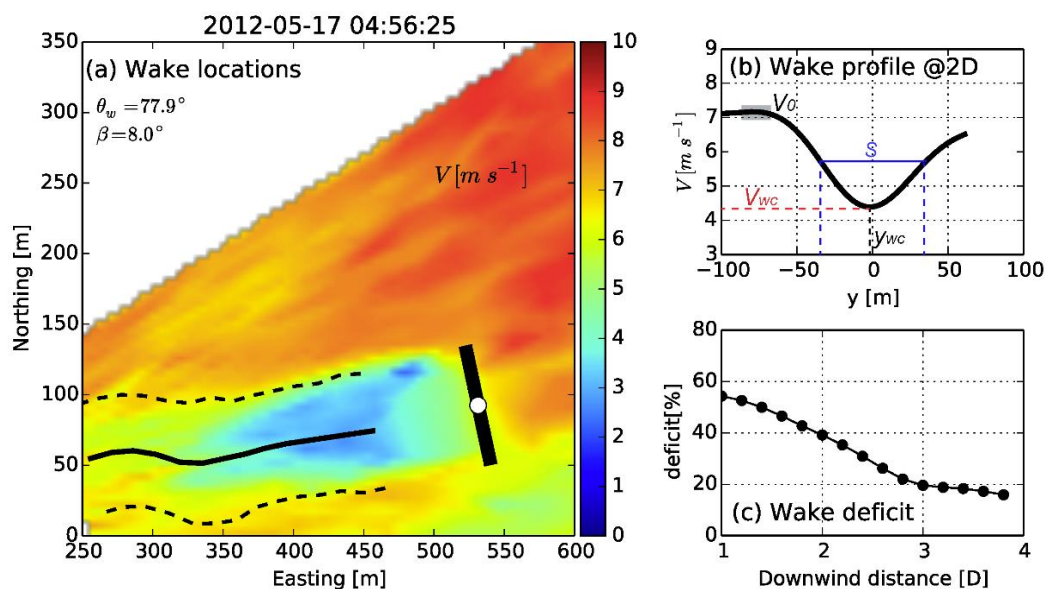


Figure 6. An example of wind speed retrieved for one stack of PPI scan. The wind speed over the entire scanned area is shown in (a). The wind turbine rotor orientation is denoted by the dark bar with a white circle indicating the location of WT2. The dark line is the wake center and the dashed lines denote the wake width. The estimated wind speed profile across the line that is parallel to the rotor plane at 2.0D downwind of WT2 is shown in (b). The definitions of wake center (y_{wc}), the FWHM (S), wake center wind speed (V_{wc}) and freestream wind speed (V_0) are also shown in (b). The wake deficit (δ in Eq. (7)) as a function of the downwind distance normalized by the rotor diameter (D) is shown in (c).

where w_{gt} is the weight assigned to the wind speed at a range gate located at (x, y) , l is the distance between the range gate and the point of interest [7]. The term L is a constant and it is set to 20 m considering that the Galion's spatial resolution is about 40 m. The distribution of the weight for a point at 2.0D downwind of WT2 is shown in Fig. 5. An example of a wake profile estimated at 2.0D downwind of WT2 is illustrated in Fig. 6b. The wake center (y_{wc}) is the location of the minimum wind speed or the wake center wind speed (V_{wc}) on the line. The wake deficit (δ) is defined as

$$\delta = \frac{V_0 - V_{wc}}{V_0} \quad (7)$$

where V_0 is the freestream wind speed which is estimated as the mean of the five highest wind speeds from the wake profile. The Full Width at Half Maximum (FWHM, and denoted as S) is used to characterize the wake width. The FWHM is estimated as the distance between the wake center and the location at which wind speed recovers by 50% (i.e. the deficit is 0.5δ). As shown in Fig. 6, the algorithm described above can detect the wake center and width up to $3.8D$ downwind of WT2. The estimated wake deficit decreases with the downwind distance from $\sim 60\%$ at $1.0D$ to $\sim 20\%$ at $3.0D$ (Fig. 6c). This is consistent with other observations [3].

5 Results and discussions

Wakes of WT2 are observed during two periods marked as wake1 and wake2 in Fig. 7, respectively, and their characteristics such as wake deficit and wake width will be presented hereafter. The wake1 period lasted for about 3 hours. WT2 was in the wake of the whole wind farm as the wind direction gradually changed from 60° to 90° . Measurements from both the cup anemometers on the meteorological mast and the ZephIR lidars were affected by the wakes of WT1 and WT2 (Fig. 7). During the wake2 period, the wind veered from 100° to 125° as the wind speed ramped up to 11 m s^{-1} . Then the wind backed to 115° and the wind speed dropped to 8 m s^{-1} . Large wind shear was also observed during this period (Fig. 7). Wake profiles derived during the wake2 period represent single wakes from WT2 because WT2 is located in the first row of the wind farm. The freestream wind speed estimated from the wake profiles matches closely with measurements from the cup anemometer and the ZephIR lidar during the wake2 period (Fig. 7).

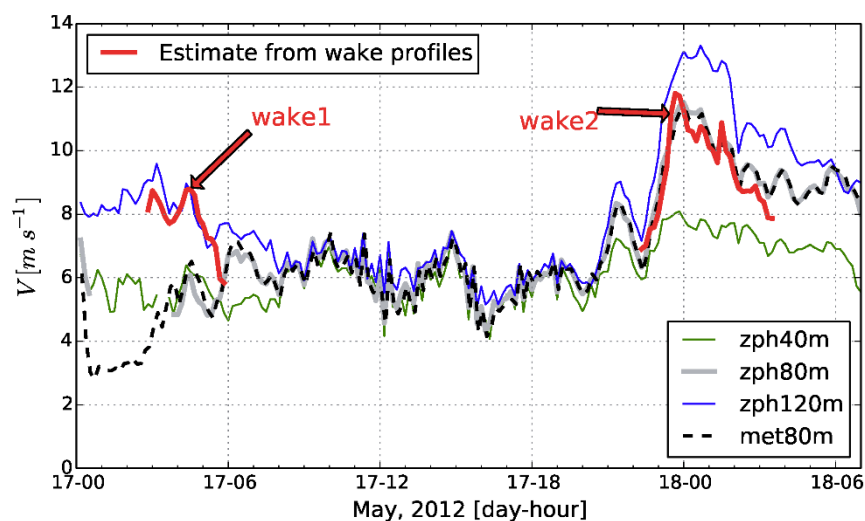


Figure 7. Time series for wind speed observed at 80 m on the meteorological mast and at 40 m, 80 m and 120 m heights by the ZephIR lidar. The two red lines are the time series of the freestream wind speed (V_0 in Eq. (7)) derived from the estimated wake profiles.

5.1 Wake deficit

Wake deficits are presented as a function of the downwind distance normalized by the rotor diameter (D) from WT2 in Fig. 8 and 9 for the wake1 and wake2 period, respectively. During the wake1 period, the lidar scanning geometry allows wake measurement up to $3.8D$ downwind of WT2. The wake deficit decreases with increasing downwind distance from $56\% \pm 4\%$ at $1.0D$ to $12\% \pm 6\%$ at $3.8D$ (Fig. 8). Note that the height at which the wake deficit is evaluated also decreases with increasing downwind distance because of the non-zero elevation angle (Fig. 8). Though the height is below the bottom tip of the rotor beyond $3.6D$ downwind of WT2, the wake deficit ($\sim 12\%$) still exists as the result of wake expansion. During the wake2 period, the lidar scanning geometry can only measure wake profiles up to $2.6D$

downwind of WT2. The height of the detected wake center remains almost the same along the downwind distance. The wake deficit has little variation between 1.0 D and 1.6D downwind of WT2 and gradually decreases with increasing downwind distance beyond 1.6D. Large variations in wake deficit are observed because WT2 was operating in a wide wind speed range ($7.5\text{--}11.5\text{ m s}^{-1}$) during this period. The thrust coefficient of WT2 is low at high wind speeds, causing the low wake deficit for cases with wind speed $> 10.5\text{ m s}^{-1}$. However, the low wake deficits observed at high wind speeds are overestimated (i.e. the wake deficit is not low enough) because of the large height variation along each wake profile and the large vertical wind shear associated with these cases (Fig. 10). For example, in the case shown in Fig. 10, the wake center is located at 65 m height with wind speed 7.1 m s^{-1} . The wake deficit is 35% based on the freestream wind speed (11 m s^{-1}) estimated as the mean of the five highest wind speeds on the wake profile. However, the estimated freestream wind speed is from 80 m height. The actual freestream wind speed at 65 m height is about 10 m s^{-1} according to the ZephIR measurement. Therefore, the actual wake deficit should be 29%, which is overestimated by 6% using the method presented in Sec. 4.4.

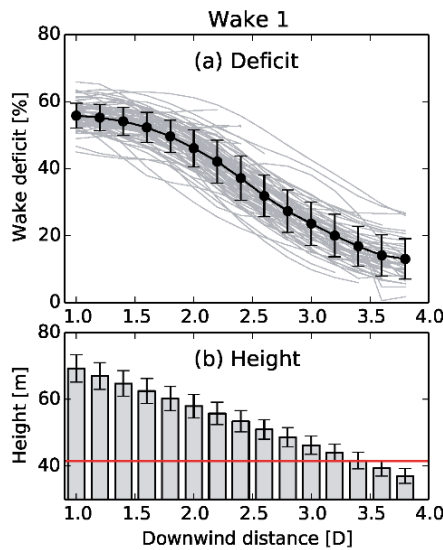


Figure 8. Wake deficit observed during the wake1 period as a function of the downwind distance in (a). The detected wake center height is given in (b) and the error bars denote the range. The red line in (b) denotes the rotor bottom tip.

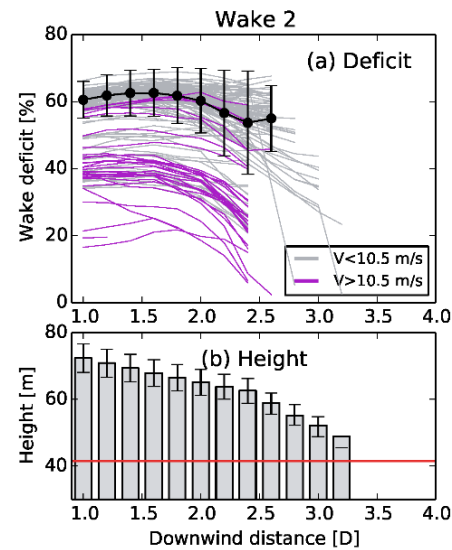


Figure 9. Wake deficit observed during the wake2 period as a function of the downwind distance in (a). The detected wake center height is given in (b) and the error bars denote the range. The red line in (b) denotes the rotor bottom tip.

5.2 Wake width

The wake width derived from the wake profile is the FWHM (S) at a height that varies with the wind direction. Assuming that the wake deficit on the cross section parallel to the rotor plane of WT2 is axisymmetric about the rotor axis, the FWHM at the hub height (S_{hub}) can be estimated by the following equation:

$$S_{hub} = \sqrt{S^2 + 4\Delta z^2} \quad (8)$$

where Δz is the height difference between the hub height and the detected wake center. By further assuming the wake deficit follows a Gaussian profile, the hub height equivalent wake width, defined as

four times the standard deviation of the Gaussian profile, is calculated as $1.7S_{hub}$ and presented in Fig. 11.

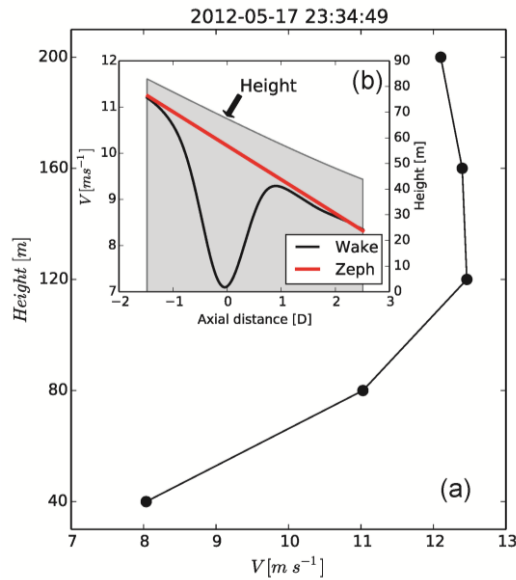


Figure 10. Wind shear measured by the ZephIR lidar in (a) and the wake profile derived from a PPI stack at 2D downwind of WT2 in (b) during the same 10-minute period. In (b), the dark line is the wake profile and the red line is the linearly interpolated from the ZephIR measurements at 40 m and 80 m in (a). The shaded area shows height variation across the wake profile.

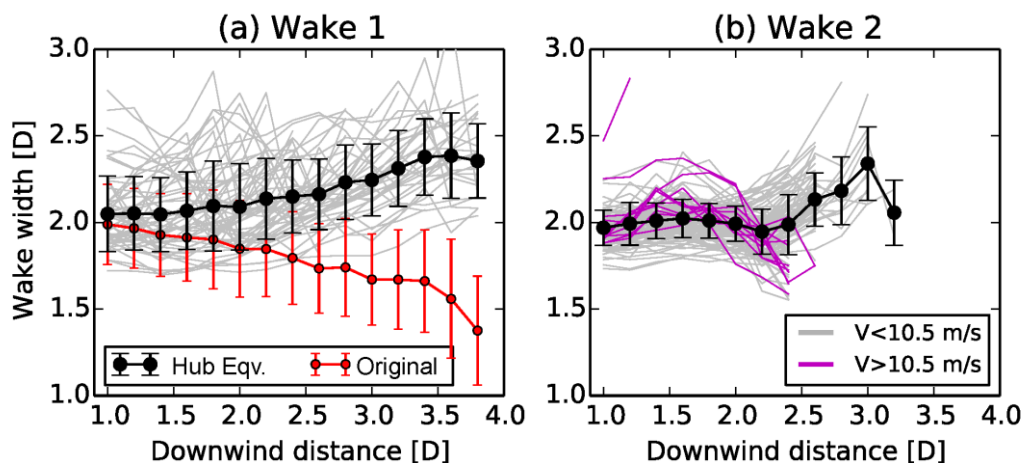


Figure 11. The equivalent hub height wake width as a function of the downwind distance normalized by the rotor diameter (D) for (a) the wake1 period and (b) the wake2 period. The gray and purple lines represent wake width estimates from individual PPI stacks for low and high wind speed cases, respectively. Error bars show the mean with plus/minus one standard deviation. The dark error bars are based on the equivalent hub height wake width and the red error bars are derived from the original wake width estimated directly from the Galion measurements. The purple lines the wake2 period are not included in calculating the error bars.

During the wake1 period, the hub height equivalent wake width on average increases from $2.0D$ to $2.3D$ along the downwind distance of WT2. However, the wake widths from some individual PPI stacks show large variability with the downwind distance, and the variability is mainly caused by the inhomogeneous wind field on the edge of the wind farm (e.g. wind speed gradient seen in Fig. 6a). The original wake width decreases with increasing downwind distance because the height of Galion measurements decreases as the wake moves away from WT2. During the wake2 period, the average wake width

remains constant (about $2.0D$) between $1.0D$ and $2.0D$ downwind of WT2. Note that wake widths during the wake2 period are derived from wake profiles on slanted lines (Fig. 10). The wake profile on a slanted line is not symmetric when the vertical wind shear is high (Fig. 10), causing difficulty in defining and detecting the wake width. The unexpected relationship between the wake width and the downwind distance for high wind speed cases (the purple lines in Fig. 11) could be the result of asymmetric wake profiles on the slanted line, and hence, should not be used to characterize the wake expansion downwind of WT2.

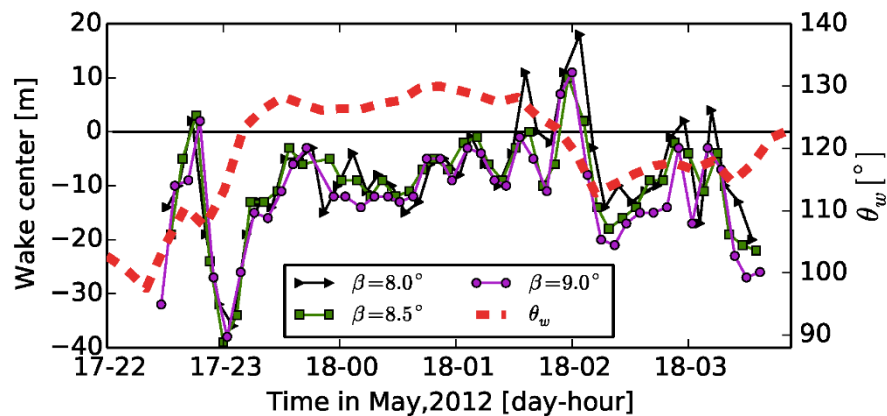


Figure 12. Time series of the estimated wake center during the wake2 period from PPI stacks with elevation angle 8.0° , 8.5° and 9.5° , respectively. The dashed red line is the time series of wind direction.

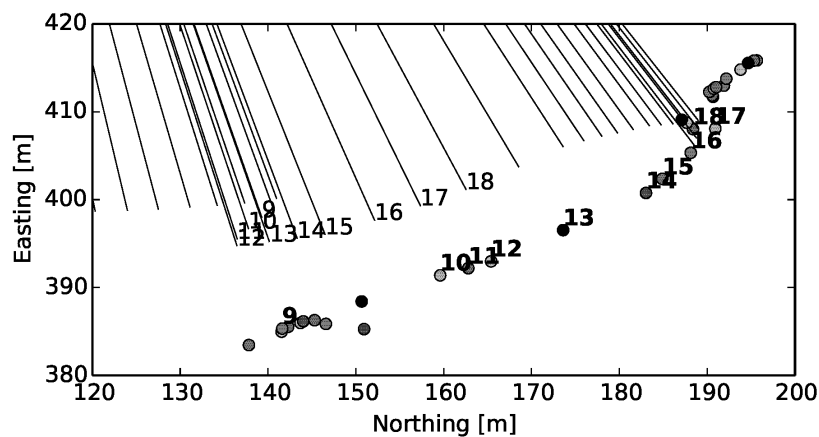


Figure 13. Locations of wake centers (circles) and wind directions (lines) observed between 22:40 and 23:59 on May 17, 2012 local time. The numbers denotes the time sequence of the wake centers and wind directions

5.3 Wake center

The time series of the wake center at $2.0D$ downwind of WT2 is shown in Fig. 12 for the wake2 period. The wake center deviates from the rotor axis by about 40 m or $0.5D$ at the beginning of this period when wind veers from 95° to 125° . Meanwhile the temporal variation of wake center is large. When the wind direction becomes more constant, the wake center becomes stationary with a constant 10 m deviation from the rotor axis for about 2 hours. Then the wake center starts to fluctuate again as a result of the changing wind direction. It is worth noting that the wake center locations shown in Fig. 12 are relative to the rotor axis of WT2 that is assumed to be parallel to the wind direction. If the wind direction is incorrect or there is a yaw error, the orientation of the rotor axis will be wrongly determined, and

consequently the deviation of the wake center from the rotor axis shown in Fig. 12 will be erroneous. The absolute wake center locations in the Galion-based coordinates system (x' , y') are plotted in Fig. 13 for the first two hours of the wake2 period. The wake center moves as the wind direction changes (shifting from left to right in Fig. 13) and the wake center only varies within 10 m when the wind direction stabilizes (see upper right corner in Fig. 13). There is always an offset between the wake center and the wind direction or the rotor axis, indicating possible wind direction errors or wind turbine yaw errors. However, neither of these errors can be verified without the operational data of WT2.

6 Conclusions

This paper presents the results from an experiment designed to measure wakes of a continuously yawing wind turbine with a ground-based coherent Doppler wind lidar in a large wind farm. Three-stack PPI scans are used. Radial velocities from the lidar are converted to wind speeds using the concurrent wind direction measurements from a meteorological mast. By assuming no yaw error of the wind turbine, wake profiles are estimated for every 0.2D downwind of the wind turbine using a weighted averaging method. Wake statistics such as wake deficit, wake width and wake center are then automatically detected from the wake profiles. Consistent with previous observations, the wake deficit decreases and the wake width increases with increasing downwind distance. The location of the wake center shows no variation with downwind distance, but its movement with changing wind direction is observed. While the lidar measurements from PPI scans can be used to automatically detect wakes from multiple directions, care must be taken with regards to the height variation over the conical surface. Depending on the wind direction or wind turbine orientation, the derived wake statistics can be contaminated by wind shear and become difficult to interpret. Hence, future work needs to seek the possibility of accounting for the height variation by incorporating three dimensional wake properties in wake profile estimate and provide practical guidelines for designing PPI scans for lidar wake measurements.

7 Acknowledgments

This project is funded by the National Science Foundation #1464383 and Department of Energy (DE EE0005379). Meanwhile, the authors gratefully acknowledge the owner of the wind farm and help from SgurrEnergy.

8 References

- [1] Barthelmie, R.J., et al., *Modelling and measuring flow and wind turbine wakes in large wind farms offshore*. Wind Energy, 2009. **12**(5): p. 431-444. DOI: 10.1002/we.348.
- [2] Barthelmie, R.J., et al., *Comparison of wake model simulations with offshore wind turbine wake profiles measured by sodar*. Journal of Atmospheric and Oceanic Technology, 2006. **23**(7): p. 888-901.
- [3] Aitken, M.L., et al., *Quantifying Wind Turbine Wake Characteristics from Scanning Remote Sensor Data*. Journal of Atmospheric and Oceanic Technology, 2014. **31**(4): p. 765-787.
- [4] Iungo, G.V. and F. Porté-Agel, *Volumetric Lidar Scanning of Wind Turbine Wakes under Convective and Neutral Atmospheric Stability Regimes*. Journal of Atmospheric and Oceanic Technology, 2014. **31**(10): p. 2035-2048.
- [5] Hirth, B.D., et al., *Coupling Doppler radar-derived wind maps with operational turbine data to document wind farm complex flows*. Wind Energy, 2015. **18**(3): p. 529-540.
- [6] Barthelmie, R.J., et al., *3D wind and turbulence characteristics of the atmospheric boundary-layer*. Bulletin of the American Meteorological Society, 2014. **95**: p. 743-756.
- [7] Daley, R., *Atmospheric data analysis*. 1993: Cambridge university press.